SCIENCE CHINA
Chemistry

•ARTICLES•

August 2020 Vol.63 No.8: 1040–1045
https://doi.org/10.1007/s11426-020-9763-9

# Enhancing the photoelectrocatalytic performance of metal-free graphdiyne-based catalyst

Ming Li[†], Hong-Juan Wang[†], Chao Zhang, Yong-Bin Chang, Sheng-Jie Li, Wen Zhang[*] & Tong-Bu Lu[*]

*International Joint Laboratory of Materials Microstructure, Ministry of Education, Institute for New Energy Materials and Low Carbon Technologies, School of Material Science and Engineering, Tianjin University of Technology, Tianjin 300384, China*

Received March 1, 2020; accepted April 29, 2020; published online May 22, 2020

As a new member of the carbon family, graphdiyne is an intrinsic semiconductor featuring a natural bandgap, which endues it potential for direct application in photoelectric devices. However, without cooperating with other active materials, conventional hexacetylene-benzene graphdiyne (HEB-GDY) shows poor performances in photocatalysis and photoelectric devices due to its non-ideal visible light absorption, low separation efficiency of the photogenerated carriers and insufficient sites for hydrogen production. Herein, we report a molecular engineering strategy for the regulation of GDY-based carbon materials, by incorporating a strong pyrene absorption group into the matrix of graphdiyne, to obtain pyrenyl graphdiyne (Pyr-GDY) nanofibers through a modified Glaser-Hay coupling reaction of 1,3,6,8-tetraethynylpyrene (TEP) monomers. For comparison, phenyl graphdiyne (Phe-GDY) nanosheets were also constructed using 1,3,4,6-tetraethynylbenzene (TEB) as a monomer. Compared with Phe-GDY, Pyr-GDY exhibits a wider visible light absorption band, promoted efficiency of the charge separation/transport and more sufficient active sites for water reduction. As a result, Pyr-GDY alone displays superior photoelectrocatalytic performance for water splitting, giving a cathode photocurrent density of ~138 μA $cm^{-2}$ at a potential of −0.1 V*versus* normal hydrogen electrode (NHE) in neutral aqueous solution, which is almost ten and twelve times as high as those of Phe-GDY (14 μA $cm^{-2}$) and HEB-GDY (12 μA $cm^{-2}$), respectively. Such a performance is also superior to those of most reported carbon-based metal-free photocathode. The results of theoretical calculations reveal that the carbon atoms in the acetylene bonds are the active sites for proton reduction. This work offers a new strategy for the construction of graphdiyne-based metal-free photoelectrocatalysts with enhanced photoelectrocatalytic performance.

**graphdiyne, metal-free photocathode, photoelectrocatalyst, water splitting**

**Citation:** Li M, Wang HJ, Zhang C, Chang YB, Li SJ, Zhang W, Lu TB. Enhancing the photoelectrocatalytic performance of metal-free graphdiyne-based catalyst. *Sci China Chem*, 2020, 63: 1040–1045, https://doi.org/10.1007/s11426-020-9763-9

## 1 Introduction

On the road to solve the problems brought by global fossil fuels, the development of clean energy is a crucial step [1]. As solar energy is the most important renewable and clean energy with huge reserves and wide distributions [2,3], the efficient conversion and utilization of solar energy is of great significance to alleviate the current energy crisis and environmental issues [4–7]. In this regard, photoelectrochemical (PEC) water splitting has attracted extensive attention due to its capability of integrating the collection of solar energy and the production of electricity and hydrogen [8–11].

Although great efforts have been dedicated to the development of photoelectrochemical cells (PECs), it is still rather challenging to simultaneously meet the requirements of cost-effective, long-term stable and high efficiency [11–13,14].

†These authors contributed equally to this work.
*Corresponding authors (email: zhangwen@email.tjut.edu.cn; lutongbu@tjut.edu.cn)

Conventional PEC photocathodes generally resort to photoactive materials such as metal oxides [15,16], silicon [17,18], metal sulfides [19,20] and copper-based chalcogenides [21]. However, the high cost and not straightforward manufacturing techniques bring about scale up restraints. In recent years, some metal-free carbon materials have emerged as promising alternatives to the abovementioned photoactive materials. The representative materials are conjugated organic materials, such as graphitic carbon nitride (g-$C_3N_4$) [22–25], covalent triazine frameworks (CTFs) [26,27], thiophenyl frameworks [28,29] and various heteroatom-free carbon frameworks [30,31], all of which demonstrate that carbon-based materials are an important class of synthetic semiconductor for the storage and conversion of solar energy. However, most of the reported metal-free carbon materials display very low hydrogen evolution reaction (HER) photocurrents (less than 50 μA $cm^{-2}$, see Table S2, Supporting Information online), due to their poor visible-light absorption ability and the lack of efficient catalytic centers. The construction of metal-free photocathodes with high HER photocurrents remains a great challenge.

Graphdiyne (GDY), which contains diacetylene links between $sp^2$-hybridizd carbon atoms, holds great promise as an optoelectronic material by virtue of its natural semiconductor bandgap. Particularly, hexacetylene-benzene graphdiyne (HEB-GDY), which was first synthesized by Li and coworkers in 2010 [32], has been widely used as a key component in the rechargeable batteries [33,34], solar cells [35,36], and photoelectric catalysis [12,13,37–40]. However, owing to its poor light-harvest ability, HEB-GDY itself shows non-ideal performance for PEC water splitting, such as only marginal hydrogen productivity and relatively low saturation cathode photocurrent density (about 20 μA $cm^{-2}$) [12,13,40].

As the microscopic structures of nanomaterials determine their physical and chemical properties [41], we are interested in the function-oriented design and engineering of GDY structure at the molecular level and exploring the catalytic active sites of such sp- and $sp^2$-hybrid carbon material. In this work, through copper surface-mediated Glaser coupling reaction [42], we used 1,3,6,8-tetraethynylpyrene (TEP) and 1,3,4,6-tetraethynylbenzene (TEB) as conjugated monomers, and synthesized 1D ultrafine GDY nanofibers (Pyr-GDY) and 2D GDY nanosheet (Phe-GDY), respectively (Scheme 1). The photoelectric test results show that compared with Phe-GDY, Pyr-GDY has a wider visible light absorption band, stronger light response and longer optical carrier lifetime. More importantly, when Pyr-GDY is used independently as a metal-free photocathode for PECs, the resulting photocurrent reaches up to 138 μA $cm^{-2}$ at −0.1 V *vs*. normal hydrogen electrode (NHE) in neutral aqueous solution (100 mW $cm^{-2}$), which is almost ten and twelve times as high as those of Phe-GDY (14 μA $cm^{-2}$) and HEB-GDY (about 12 μA $cm^{-2}$), respectively. Such a performance is also superior to those of most reported metal-free photocathode materials (Table S2). The results of density functional theory (DFT) calculation revealed that the carbon atoms in the acetylene bonds are the active sites for proton reduction.

## 2 Experimental

### 2.1 Instruments and method

Ultraviolet-visible (UV-Vis) absorption spectra were measured by an UV-Vis-NIR spectrophotometer (Lambda 750, PerkinElmer, USA). Raman spectra were detected by a laser confocal fiber Raman spectrometer (HORIBA EVOLVTION, HORIBA JobinYvon, France). X-ray photo-electron spectroscopy (XPS) measurements were conducted on an ESCALAB 250 Xi spectrometer (Thermo Scientific, USA) with Al-Kα as the excitation source. Transmission electron microscope (TEM) images were obtained on Talos F200X, FEI (USA) using 120 kV acceleration voltage. Gas product was detected on GC-2014 (Shimadzu, Japan).

### 2.2 Photoelectrochemical measurements

All electrochemical tests were carried out in a three-electrode system with a reference electrode of Ag/AgCl and a counter electrode of Pt. The simulated sunlight came from a 300 W xenon lamp (100 mW $cm^{-2}$). The electrolyte 0.1 M $Na_2SO_4$ (pH 6.8) was deoxygenated by pumping argon at room temperature (about 25 °C) for 20 min before measurement. The linear sweep voltammetry (LSV) characteristics of the electrodes were measured using an electrochemical analyzer (CHI 660 E) at a scan rate of 2 mV $s^{-1}$. The electrochemical impedance spectrum (EIS) was recorded by applying a 50 mV alternating current (AC) signal over a frequency range of $10^5$ to 0.1 Hz at a bias of 0.197 V *vs*. NHE on PGSTAT 302N (Metrohm).

### 2.3 Preparation of Pyr-GDY and Phe-GDY

Pyr-GDY and Phe-GDY were synthesized with similar procedures (as shown in Scheme 1, and Schemes S1 and S2, Supporting Information online). In brief, clean Cu foils were immersed in a mixed solution of acetone (100 mL), pyridine (5 mL) and tetramethylethylenediamine (1 mL). After desilication, TEP/TEB monomer dissolved in acetone was slowly added into the above solution and heated at 50 °C for 12 h. The copper ions released from Cu foils acted as the catalyst for the coupling reactions of terminal alkynes [43,44], and the terminal alkynes of TEP/TEB could couple with each other to form extended π-conjugated carbon skeletons containing butadiyne links and pyrene/benzene rings

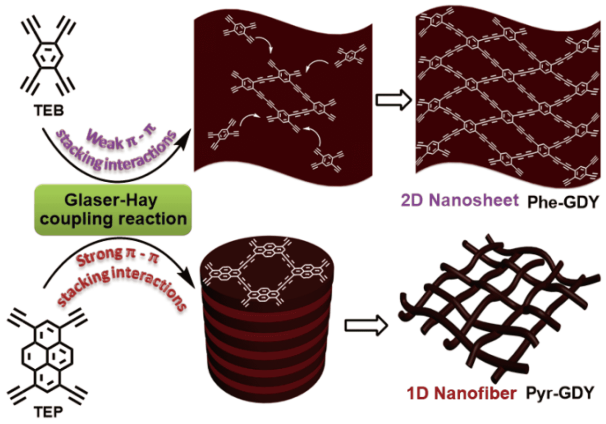


**Scheme 1** Illustration of the synthesis processes for Pyr-GDY and Phe-GDY (color online).

(Scheme 1). As a result, two brown films (Pyr-GDY and Phe-GDY) were grown on the copper foil with high structural stability and good mechanical adhesion (Figure S1, Supporting Information online), and the films were directly used as the photocathodes.

## 3 Results and discussion

### 3.1 Characterization of Pyr-GDY and Phe-GDY

The TEM images of Pyr-GDY and Phe-GDY in Figure 1 show that Pyr-GDY presents a network texture of interwoven 1D fibers, and the diameters of these nanofibers are about 20 nm (Figure 1(a)). In comparison, the morphology of Phe-GDY is stacked 2D nanosheets (Figure 1(b)), analogous to that of the classical HEB-GDY [32]. Apparently, the nanotopography of Pyr-GDY is in favor of the full exposure of its active sites in electrolyte surface, and conducive to the release of generated hydrogen in the PECs. Herein, the difference in morphology between Pyr-GDY and Phe-GDY is presumably due to the strong π-π stacking interactions among TEP monomers; small pieces of Pyr-GDY are prone to stack along the perpendicular direction to form 1D nanofibers. In addition, the XRD patterns and high resolution TEM (HRTEM) image of Pyr-GDY (Figures S2 and S3) clearly show the interlayer spacing around 0.37 nm, in consistent with the above inference. By contrast, the π-π stacking interactions between TEB monomers are relatively weak, and thus the alkyne coupling reactions along the 2D planar directions are favored, resulting in the formation of 2D Phe-GDY nanosheets (Scheme 1). These results indicate that even under the same synthesis conditions, the nanostructures of GDY can be regulated at the molecular level by selecting different starting monomers.

The chemical compositions and electronic structures of Pyr-GDY and Phe-GDY were investigated by XPS and Raman spectroscopy. As shown in Figure 1(d), Pyr-GDY and Phe-GDY are both composed mainly of carbon element. The existence of oxygen is probably due to the adsorption of oxygen or partial oxidation of the acetylene bonds by the oxygen in ambient atmosphere [12,32]. The C 1s peaks in the XPS spectra of Pyr-GDY and Phe-GDY show four similar components (Figure 1(e, f)), which are assigned to C≡C (sp), C=C ($sp^2$), C–O, and C=O, respectively [32]. Besides, the integration ratio of sp and $sp^2$ hybridized carbons in Pyr-GDY and Phe-GDY are about 0.5 and 1.3 (Table S1), consistent with the structures of TEP and TEB monomers, respectively. In addition, the Raman spectra of Pyr-GDY and Phe-GDY show two characteristic peaks around 1,900 and 2,100 $cm^{-1}$ (Figure 1(c)), which are ascribed to the vibration of conjugated diacetylene links [32,42,45]. The above experimental results indicate that Pyr-GDY and Phe-GDY were successfully constructed by the C–C coupling reaction of terminal alkynes.

In order to examine the photoredox properties of Pyr-GDY and Phe-GDY, the electronic band structures of these two nanostructures were characterized by UV-Vis absorption spectroscopy, XPS and ultraviolet photoelectron spectroscopy (UPS). The absorption spectra of TEP and TEB monomers in Figure S4 show that TEP has a wider absorption band in visible light region than TEB. Similarly, compared with Phe-GDY, Pyr-GDY also has a wider absorption band in visible light region. The absorption edge of Pyr-GDY and Phe-GDY are round 700 and 600 nm, respectively (Figure 2(a)). Correspondingly, the optical bandgap ($E_{BG}$)

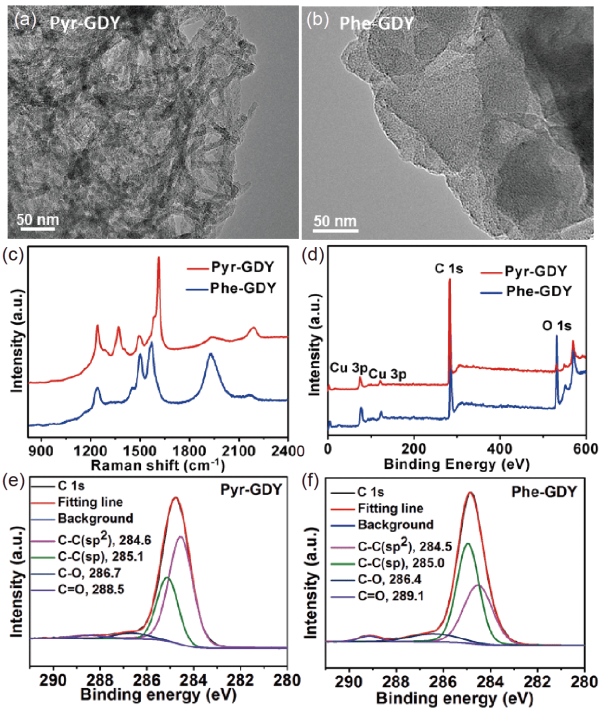


**Figure 1** TEM images of Pyr-GDY (a) and Phe-GDY (b); Raman spectra (c) and XPS survey spectra (d) of Pyr-GDY and Phe-GDY; high-resolution XPS spectra of C 1s of Pyr-GDY (e) and Phe-GDY (f) (color online).

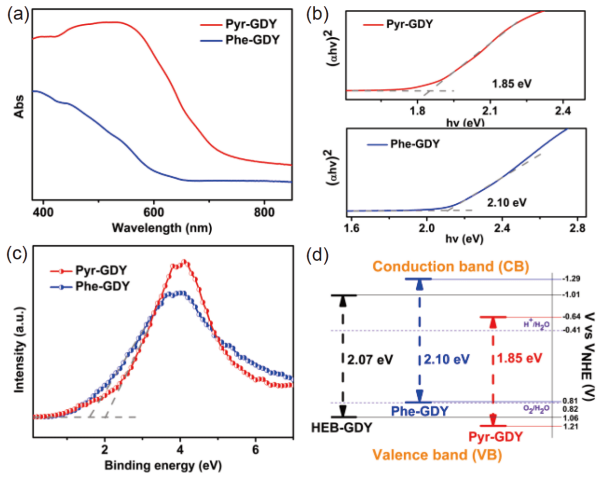


**Figure 2** UV-Vis absorption spectra of (a) Pyr-GDY and Phe-GDY; (b) the Tauc polts of $(\alpha hv)^2$ *versus* photo-energy for Pyr-GDY and Phe-GDY; (c) XPS valence spectra of Pyr-GDY and Phe-GDY; (d) band structures of Pyr-GDY, Phe-GDY and HEB-GDY (color online).

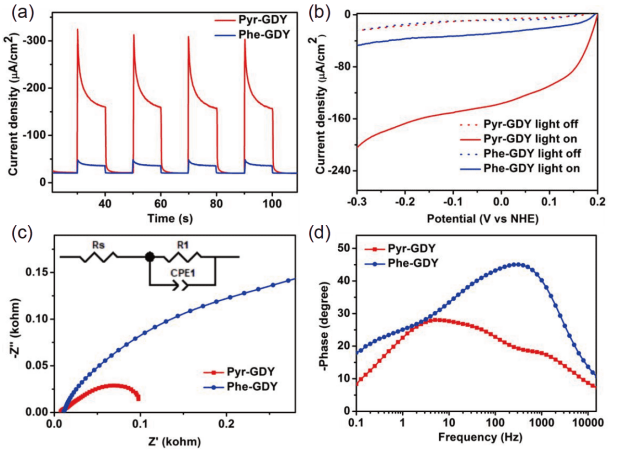


**Figure 3** PEC characterizations. (a) Plot of current density *versus* time of Pyr-GDY and Phe-GDY under intermittent irradiation; (b) LSV of Pyr-GDY (red) and Phe-GDY (blue) as photocathodes measured under dark and light; (c) the electrochemical impedance spectra and the equivalent circuit of Pyr-GDY and Phe-GDY measured under light; (d) the Bode phase plots of Pyr-GDY and Phe-GDY (color online).

values of Pyr-GDY and Phe-GDY evaluated from UV-Vis spectra are ~1.85 and ~2.10 eV, respectively (Figure 2(b)). Then, UPS was conducted to estimate the HOMO position of Pyr-GDY (Figure S5) [12]. As a result, the valence band (VB) position of Pyr-GDY was obtained as 1.21 V *vs*. NHE. In addition, the VB of Phe-GDY can be calculated from the valence band difference between Pyr-GDY (2.0 eV) and Phe-GDY (1.6 eV) (Figure 2(c)) as 0.81 V *vs*. NHE. The conduction bands (CB) of Pyr-GDY and Phe-GDY were calculated ($E_{VB}$–$E_{BG}$) to be −0.64 and −1.29 V *vs*. NHE, respectively. According to the above results, the band structures of Pyr-GDY, Phe-GDY and HEB-GDY [13] can be obtained (Figure 2(d)). The results show that the CB potential of Pyr-GDY is more negative than that of the hydrogen electrode, and its VB potential is more positive than that of the oxygen electrode. By contrast, for Phe-GDY, the VB potential was slightly above that of the oxygen electrode, which was disadvantageous for water oxidation. Besides, the $E_{BG}$ values of Phe-GDY and HEB-GDY were larger than that of Pyr-GDY, suggesting that higher photon energies are needed to generate carriers in these two materials. Thus, the proper band position and energy gap may enable the Pyr-GDY nanofibers to work as a superior photoelectrode material for PEC devices.

### 3.2 Photoelectrocatalytic performances of Pyr-GDY and Phe-GDY photocathodes

In order to assess the PECs performances of these two GDY-based materials, Pyr-GDY and Phe-GDY grown on the copper substrate were used directly as photocathodes in $Na_2SO_4$ solution (pH 6.8). As shown in Figure 3(a), both Pyr-GDY and Phe-GDY showed response to light switch at −0.1 V *vs*. NHE (the light intensity is 100 mW cm$^{-2}$), suggesting that Pyr-GDY and Phe-GDY display typical p-type semiconductor behavior. Particularly, Pyr-GDY showed a much higher saturated cathodic photocurrent than Phe-GDY (Figure 3(a)) and HEB-GDY (Figure S6(b)). The cathodic photocurrent density of Pyr-GDY was approximately 138 μA cm$^{-2}$, almost ten and twelve times as high as those of Phe-GDY (14 μA cm$^{-2}$) and HEB-GDY (about 12 μA cm$^{-2}$) after subtracting the dark current. This performance is also superior to most of the reported metal-free and non-composite photoelectrodes, such as classical GDY, graphite carbon nitride, and other carbon-based photocathode materials (see Table S2). The LSV curves of Pyr-GDY, Phe-GDY and HEB-GDY under dark and light conditions also showed that Pyr-GDY exhibits a relatively higher light response current than Phe-GDY (Figure 3(b)) and HEB-GDY (Figure S6(a)) at different bias. In addition, the EIS measurements in Figure 3(c) show that compared with Phe-GDY, Pyr-GDY has a much lower arc radius under light illumination. Besides, the charge-transfer resistances calculated with an equivalent circuit (inset in Figure 3(c)) are 135.4 and 709.8 Ω for Pyr-GDY and Phe-GDY, respectively, suggesting that the charge transport resistance of Pyr-GDY was lower than that of Phe-GDY. Furthermore, the electron lifetime of Pyr-GDY and Phe-GDY can be obtained from the Bode phase plots (Figure 3(d)) [46,47]. The maximum frequencies ($f_{max}$) of Pyr-GDY and Phe-GDY were measured to be 5 and 316 Hz, respectively. As a result, the calculated electron lifetime of Pyr-GDY ($3.17\times10^{-2}$ s) was almost 63 times as long as that of Phe-GDY ($5.04\times10^{-4}$ s), indicating that the recombination of photogenerated carriers in Pyr-GDY is much slower, and the carrier transfer kinetics of Pyr-GDY was superior to that of Phe-GDY. Here, the mechanisms for the enhanced charge transfer of Pyr-GDY are mainly

ascribed to these three aspects: wider light absorption property, proper band structure and elaborated nanostructure. These advantages may corporately result in the enhancement of the charge transfer in Pyr-GDY. In addition, the electrolysis experiment suggested that after 0.73 C charge passed through the external circuit, an approximately 3.4 μmol of $H_2$ was produced, and the corresponding Faraday efficiency was up to 90%. Besides, the incident photon-to-current efficiency (IPCE) measurements (Figure S7) show that Pyr-GDY photocathode has a higher IPCE value (1.1%) than that of Phe-GDY (0.2%) at 525 nm. To evaluate the stability of the Pyr-GDY photocathode, scanning electron microscope (SEM), Raman spectroscopy measurements and electrolysis on Pyr-GDY were tested (Figures S8–S10). The results showed that after photoelectrolysis for 5 h, the morphology, Raman peaks and electrolysis current of Pyr-GDY were similar to those before photoelectric reaction, demonstrating the good stability of Pyr-GDY as photocathode material.

### 3.3 DFT calculations

To gain more in-depth insight on the real HER-active sites of these two graphdiyne-based materials, the Gibbs free energies for hydrogen adsorption on Pyr-GDY and Phe-GDY were calculated *via* DFT calculations. Specifically, the Gibbs free energies for hydrogen adsorption on seven different carbon atoms of Pyr-GDY (Figure 4(a), Figure S11) were calculated. The results in Figure 4(a) show that compared with the other carbon atoms, site 2 (acetylenic carbon next to the $sp^2$-hybrid carbon) featured a much lower Gibbs free energy of 0.630 eV for $H_2$ evolution. For Phe-GDY (Figure 4 (b), Figure S12), the DFT calculation results also show that the acetylenic carbon next to the benzene ring is a favorable site for proton adsorption and reduction. All these results indicate that the main active sites of such graphdiyne-based carbon materials for $H_2$ production are the acetylenic carbon atoms adjacent to the $sp^2$-hybrid carbon. Therefore, the graphdiyne-based materials are expected to exhibit unique advantages for hydrogen regeneration in the field of energy conversion.

## 4 Conclusions

In conclusion, we demonstrate the molecular engineering of the nanostructures of GDY by manipulating the conjugated structures of the building blocks. Specifically, by taking advantage of the different π-π stacking interactions between TEP and TEB monomers, we successfully constructed 1D Pyr-GDY ultrafine nanofibers and 2D Phe-GDY nanosheets. Because of the wider range of visible light absorption, proper band position and sufficient electrocatalytic active surface, Pyr-GDY can be used directly as a metal-free photocathode

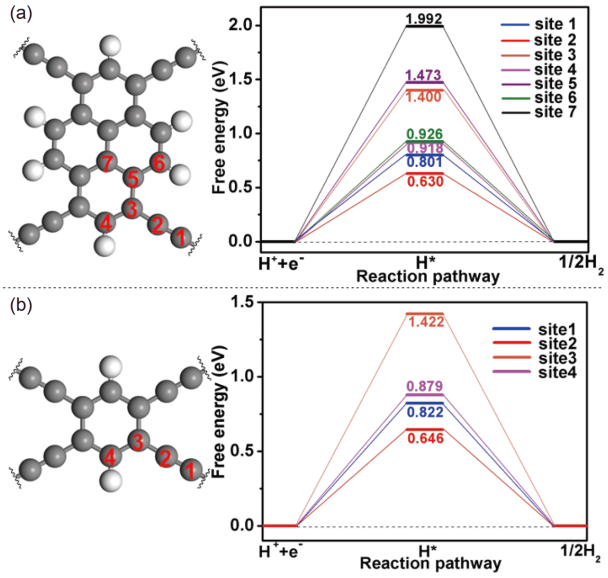


**Figure 4** The computational models and the corresponding free energy diagrams for $H_2$ evolution on different active sites of Pyr-GDY (a) and Phe-GDY (b). The grey and white balls represent C and H atoms, respectively (color online).

in PECs for $H_2$ production, delivering a saturated photocurrent of approximately 138 μA $cm^{-2}$ at −0.1 V *vs.* NHE, which was almost ten times as high as that of Phe-GDY (14 μA $cm^{-2}$), and superior to most reported metal-free and non-composite photoelectrodes, such as classical GDY, graphite carbon nitride, and other carbon-based photocathode materials. Beyond this work, we believe that through the modulation of its special electron structures, graphdiyne-based carbon materials can also serve as surprising candidates for other photo/optoelectronic devices. To sum up, our strategy here offers new in-depth insights on the relationship between the electronic structure and photoelectric properties of graphdiyne, and highlights the promising application of graphdiyne-based carbon materials as high-activity organic photoelectrodes.

**Acknowledgements** This work was supported by the National Key R&D Program of China (2017YFA0700104), the National Natural Science Foundation of China (21790052, 21702146, 21805207) and 111 Project of China (D17003).

**Conflict of interest** The authors declare no conflict of interest.

**Supporting information** The supporting information is available online at http://chem.scichina.com and http://link.springer.com/journal/11426. The supporting materials are published as submitted, without typesetting or editing. The responsibility for scientific accuracy and content remains entirely with the authors.

1 Kittner N, Lill F, Kammen DM. *Nat Energy*, 2017, 2: 17125
2 Lewis NS. *Science*, 2016, 351: aad1920
3 Kabir E, Kumar P, Kumar S, Adelodun AA, Kim KH. *Renew Sustain Energy Rev*, 2018, 82: 894–900

4 Zou X, Zhang Y. *Chem Soc Rev*, 2015, 44: 5148–5180
5 Ran J, Zhang J, Yu J, Jaroniec M, Qiao SZ. *Chem Soc Rev*, 2014, 43: 7787–7812
6 Wu LZ, Chen B, Li ZJ, Tung CH. *Acc Chem Res*, 2014, 47: 2177–2185
7 Li B, Si Y, Zhou BX, Fang Q, Li YY, Huang WQ, Hu W, Pan A, Fan X, Huang GF. *ACS Appl Mater Interfaces*, 2019, 11: 17341–17349
8 Youngblood WJ, Lee SHA, Kobayashi Y, Hernandez-Pagan EA, Hoertz PG, Moore TA, Moore AL, Gust D, Mallouk TE. *J Am Chem Soc*, 2009, 131: 926–927
9 Fujishima A, Honda K. *Nature*, 1972, 238: 37–38
10 Jiang C, Moniz SJA, Wang A, Zhang T, Tang J. *Chem Soc Rev*, 2017, 46: 4645–4660
11 Bellani S, Antognazza MR, Bonaccorso F. *Adv Mater*, 2019, 31: 1801446
12 Li J, Gao X, Liu B, Feng Q, Li XB, Huang MY, Liu Z, Zhang J, Tung CH, Wu LZ. *J Am Chem Soc*, 2016, 138: 3954–3957
13 Han YY, Lu XL, Tang SF, Yin XP, Wei ZW, Lu TB. *Adv Energy Mater*, 2018, 8: 1702992
14 Li YY, Si Y, Han EX, Huang WQ, Hu W, Pan A, Fan X, Huang GF. *J Phys D-Appl Phys*, 2019, 53: 015502
15 Paracchino A, Laporte V, Sivula K, Grätzel M, Thimsen E. *Nat Mater*, 2011, 10: 456–461
16 Click KA, Beauchamp DR, Huang Z, Chen W, Wu Y. *J Am Chem Soc*, 2016, 138: 1174–1179
17 Ding Q, Meng F, English CR, Cabán-Acevedo M, Shearer MJ, Liang D, Daniel AS, Hamers RJ, Jin S. *J Am Chem Soc*, 2014, 136: 8504–8507
18 Cox CR, Lee JZ, Nocera DG, Buonassisi T. *Proc Natl Acad Sci USA*, 2014, 111: 14057–14061
19 Luo J, Tilley SD, Steier L, Schreier M, Mayer MT, Fan HJ, Grätzel M. *Nano Lett*, 2015, 15: 1395–1402
20 Chae SY, Park SJ, Han SG, Jung H, Kim CW, Jeong C, Joo OS, Min BK, Hwang YJ. *J Am Chem Soc*, 2016, 138: 15673–15681
21 Paracchino A, Mathews N, Hisatomi T, Stefik M, Tilley SD, Grätzel M. *Energy Environ Sci*, 2012, 5: 8673–8681
22 Zhang J, Li Y, Li J, Zhao Z, Liu X, Li Z, Han Y, Hu J, Chen A. *Powder Tech*, 2013, 246: 356–362
23 Wang X, Maeda K, Thomas A, Takanabe K, Xin G, Carlsson JM, Domen K, Antonietti M. *Nat Mater*, 2009, 8: 76–80
24 Zheng D, Cao XN, Wang X. *Angew Chem Int Ed*, 2016, 55: 11512–11516
25 Li B, Si Y, Fang Q, Shi Y, Huang WQ, Hu W, Pan A, Fan X, Huang GF. *Nano-Micro Lett*, 2020, 12: 52
26 Wang K, Yang LM, Wang X, Guo L, Cheng G, Zhang C, Jin S, Tan B, Cooper A. *Angew Chem Int Ed*, 2017, 56: 14149–14153
27 Vyas VS, Haase F, Stegbauer L, Savasci G, Podjaski F, Ochsenfeld C, Lotsch BV. *Nat Commun*, 2015, 6: 8508
28 Zhang T, Hou Y, Dzhagan V, Liao Z, Chai G, Löffler M, Olianas D, Milani A, Xu S, Tommasini M, Zahn DRT, Zheng Z, Zschech E, Jordan R, Feng X. *Nat Commun*, 2018, 9: 1140
29 Sun H, Öner IH, Wang T, Zhang T, Selyshchev O, Neumann C, Fu Y, Liao Z, Xu S, Hou Y, Turchanin A, Zahn DRT, Zschech E, Weidinger IM, Zhang J, Feng X. *Angew Chem Int Ed*, 2019, 58: 10368–10374
30 Wang L, Wan Y, Ding Y, Wu S, Zhang Y, Zhang X, Zhang G, Xiong Y, Wu X, Yang J, Xu H. *Adv Mater*, 2017, 29: 1702428
31 Sprick RS, Jiang JX, Bonillo B, Ren S, Ratvijitvech T, Guiglion P, Zwijnenburg MA, Adams DJ, Cooper AI. *J Am Chem Soc*, 2015, 137: 3265–3270
32 Li G, Li Y, Liu H, Guo Y, Li Y, Zhu D. *Chem Commun*, 2010, 46: 3256–3258
33 Shang H, Zuo Z, Yu L, Wang F, He F, Li Y. *Adv Mater*, 2018, 30: 1801459
34 Du H, Yang H, Huang C, He J, Liu H, Li Y. *Nano Energy*, 2016, 22: 615–622
35 Xiao J, Shi J, Liu H, Xu Y, Lv S, Luo Y, Li D, Meng Q, Li Y. *Adv Energy Mater*, 2015, 5: 1401943
36 Du H, Deng Z, Lü Z, Yin Y, Yu LL, Wu H, Chen Z, Zou Y, Wang Y, Liu H, Li Y. *Synth Met*, 2011, 161: 2055–2057
37 Lu X, Han Y, Lu T. *Acta Phys-Chim Sin*, 2018, 34: 1014–1028
38 Xing C, Xue Y, Huang B, Yu H, Hui L, Fang Y, Liu Y, Zhao Y, Li Z, Li Y. *Angew Chem*, 2019, 131: 14035–14041
39 Gao X, Li J, Du R, Zhou J, Huang MY, Liu R, Li J, Xie Z, Wu LZ, Liu Z, Zhang J. *Adv Mater*, 2017, 29: 1605308
40 Lv JX, Zhang ZM, Wang J, Lu XL, Zhang W, Lu TB. *ACS Appl Mater Interfaces*, 2019, 11: 2655–2661
41 Zhou BX, Ding SS, Zhang BJ, Xu L, Chen RS, Luo L, Huang WQ, Xie Z, Pan A, Huang GF. *Appl Catal B-Environ*, 2019, 254: 321–328
42 Zhou J, Gao X, Liu R, Xie Z, Yang J, Zhang S, Zhang G, Liu H, Li Y, Zhang J, Liu Z. *J Am Chem Soc*, 2015, 137: 7596–7599
43 Zhang T, Du Y, Kalbacova J, Schubel R, Rodriguez RD, Chen T, Zahn DRT, Jordan R. *Polym Chem*, 2015, 6: 8176–8183
44 Zhang T, Du Y, Müller F, Amin I, Jordan R. *Polym Chem*, 2015, 6: 2726–2733
45 Yang LL, Wang HJ, Wang J, Li Y, Zhang W, Lu TB. *J Mater Chem A*, 2019, 7: 13142–13148
46 Jang YH, Xin X, Byun M, Jang YJ, Lin Z, Kim DH. *Nano Lett*, 2012, 12: 479–485
47 Lu YR, Yin PF, Mao J, Ning MJ, Zhou YZ, Dong CK, Ling T, Du XW. *J Mater Chem A*, 2015, 3: 18521–18527